

Regulation of mixotrophy in *Synechocystis* by a rhomboid protease

Iskander M. Ibrahim¹, Dale Harrison², Modesta Blunskyte-Hendley³, Bill T. Ferrara² and Elinor P. Thompson^{2*}

*ORCID*s:

Modesta Blunskyte-Hendley, <https://orcid.org/0000-0002-0287-7020>

Bill T. Ferrara, <https://orcid.org/0000-0002-2163-4032>

Iskander M. Ibrahim, <https://orcid.org/0000-0002-2744-6307>

Elinor P. Thompson, <https://orcid.org/0000-0002-6434-9290>

¹Department of Biological Sciences, University of Towson, Maryland, 21252, USA.

²Faculty of Engineering and Science, University of Greenwich, Chatham Maritime, Kent, ME4 4TB, UK.

³UK Dementia Research Institute, University College London, Gower Street, London WC1E 6BT, UK.

Elinor P. Thompson

te30@gre.ac.uk

Keywords: rhomboid protease, serine protease, *Synechocystis*, CO₂-concentration mechanism, FtsH, mixotrophy

1. Abstract

The intramembrane 'rhomboid' protease family is almost ubiquitous across evolution, with its well-conserved transmembrane domains typified in crystal structures of bacterial representatives, such as the Escherichia coli GlpG. In contrast with accumulating data on

Company Limited by Guarantee | Registered in England No. 10

39582 | Registered Office Charles Darwin House, 12 Roger Street, WC1N 2JU, UK
Registered as a Charity: 264017 (England & Wales); SC039250 (Scotland)

Ibrahimslr1461Microbiology 150126f (2)

29 *rhomboid function in higher organisms, where roles in human disease are in incentive to*
30 *study, findings remain sparse about the functions and substrates of the prokaryotic enzymes,*
31 *even though these provided the earliest protein structures. In particular, nothing at all is*
32 *known about the rhomboid proteases of photosynthetic prokaryotes despite the importance of*
33 *cyanobacteria as relatives of the progenitor of chloroplasts. Findings relating to the*
34 *cyanobacterial enzymes would complement data on plant plastid rhomboids from work in*
35 *Arabidopsis thaliana. Synechocystis sp. PCC 6803 was used, therefore, to investigate*
36 *conserved photosynthetic functions across evolution for this protein family. Reverse-genetics*
37 *studies using Slr1461, the single rhomboid protease of Synechocystis 6803, did not reveal a*
38 *nonphotochemical quenching phenotype as observed for the Arabidopsis RBL10 null mutant*
39 *which lacked a chloroplast outer membrane rhomboid. The Slr1461 mutant exhibited a*
40 *marginal change in pigment composition and its growth rate was only slightly different from*
41 *WT under optimal light intensity. The most dramatic effect of inactivation of Slr1461 was the*
42 *mutant's distinct inability to reduce photosynthetic activity under mixotrophic conditions.*
43 *Concurrent phototrophy and heterotrophy in mixotrophic growth aids survival and*
44 *competitiveness in phytoplankton, allowing conservation of energy by reducing the need for*
45 *uptake and fixing of CO₂ when an organic carbon source is available. It was notable*
46 *therefore that, in the absence of the Slr1461 rhomboid, the steady-state mRNA levels were*
47 *reduced for a subset of genes encoding facilitators of high-affinity CO₂ import and of*
48 *transcriptional regulators of the carbon-concentrating mechanism (CCM). Slr1461 activity*
49 *was also linked with that of another membrane protease, the AAA protease FtsH2, which was*
50 *likewise observed to act within regulatory networks for the cyanobacterial carbon uptake*
51 *mechanism. Aberrant transcript levels were most evident specifically under high CO₂*
52 *conditions, when the impact of Slr1461 enzymatic activity appeared to be upstream of NdhR,*
53 *a central, controlling transcription factor of the CCM.*

54

55 **2. Introduction**

56 The membrane-located families were the most recently discovered group of proteases, and
57 investigations of the large 'rhomboid' group quickly proved their importance across diverse
58 cellular processes in all kingdoms of life. They are ubiquitous across evolution, rhomboid
59 proteases being found in prokaryotic to eukaryotic microbes, with organellar members in
60 mitochondria and plastids, and occurring in the metazoa [1]. Although this early paradigm
61 has become less fixed with accumulating research, a typical rhomboid substrate is typically a
62 single transmembrane protein located in the lipid bilayer, from which proteolysis releases an
63 activated peptide. A well-researched example of this is *Drosophila* Rhomboid (Rho)-1, which
64 releases epidermal growth factor (EGF) receptor for signalling [2]. Substrate and enzyme are
65 initially localised separately, on endoplasmic reticulum (ER) and Golgi apparatus,
66 respectively [3], a mechanism that prevents cleavage of the substrate, Spitz, until it is
67 trafficked to the ER.

68 Accumulating evidence for a more diverse repertoire for rhomboid action was presaged by an
69 atypical mode of action observed when an activated intermediate was found to be retained in
70 the membrane [4] (rather than released of an activated peptide) in the case of the *Providencia*
71 *stuartii* AarA rhomboid protease. In that case, quorum signalling was permitted following
72 AarA activation of the membrane-located TatA component of the Tat transport channel by
73 cleaving the N-terminal six amino acids [5].

74 Rhomboid proteases are atypical serine proteases whose conserved structure of a six- or
75 seven-transmembrane domain core contains only a catalytic dyad, comprising Ser and His
76 without the usual third active-site residue, Asp [6, 7]. Whereas crystal structures were
77 resolved of the *Haemophilus influenzae* and *Escherichia coli* bacterial enzymes, the roles of
78 prokaryotic rhomboids are only slowly being elucidated [8]. A hypothesis that *E. coli* GlpG
79 may facilitate fatty acid utilisation, enhancing survival in intestinal mucus [9], does
80 correspond with other links between rhomboids and lipids. For example, both the
81 *Corynebacterium glutamicum* [10] and *Shigella sonnei* rhomboid pairs were suggested to
82 affect membrane quality control [11] whereas two organellar rhomboid proteases were
83 hypothesised to regulate membrane-fusion dynamics, in the mitochondria of *Saccharomyces*
84 *cerevisiae* and *Drosophila melanogaster* [12, 13].

85 Another eukaryotic, organellar representative is the presenilin-associated rhomboid-like
86 (PARL) protease of the inner mitochondrial membrane, an enzyme that operates within
87 human mitochondrial-disease networks [14]. Rhomboid proteins also have medical
88 significance in their regulation of host-cell infection in the apicomplexan genera *Toxoplasma*
89 and *Plasmodium* [15, 16].

90 A catalytically inactive subset of rhomboids (iRhoms, or pseudoproteases), which lack
91 protease active-site residues, can still play roles in signal transduction. For example,
92 overexpression of *Drosophila* iRhom inhibited EGF receptor-mediated signalling [17],
93 whereas human iRhom2 is required for trafficking and activation of the tumour necrosis
94 factor (TNF)- α -converting enzyme for TNF signalling [18].

95 One or two rhomboid genes, only, tend to be found within prokaryote genomes, whereas
96 plant genomes encode multigene families of the proteases [19] but few, again, have been
97 studied. Given the prokaryotic origin of eukaryotic organelles, investigating the chloroplast
98 or mitochondrial rhomboid proteases of plants might allow evolutionary links in the enzyme
99 family to be revealed. This type of parallel study was useful for chloroplast versus
100 cyanobacterium FtsH-family membrane proteases, with *Arabidopsis thaliana* VAR2 and
101 *Synechocystis* sp. PCC 6803 Slr0228 (FtsH2) enzymes, both discovered to be operating in the
102 Photosystem II (PSII) D1 protein replacement cycle [20, 21]. Compared with four of 12 FtsH
103 enzymes thought to function in *A. thaliana* plastids [22, 23], three of about 20 rhomboid
104 proteins in the plant were so far demonstrated experimentally to be targeted to organelles. In
105 transient assays, *Arabidopsis* At1g18600 (RBL12) was observed in the mitochondria,
106 although this protein did not complement yeast mitochondrial RBD mutant function [24].
107 *Arabidopsis* At5g25752 (RBL11) was directed to the chloroplast [25], where it was

108 hypothesised to function in plastid-protein translocation [26]. A stably transformed RBL10-
109 GFP reporter was visualised in the chloroplast outer membrane, and *rbll0* null-mutants
110 demonstrated floral abnormalities, reduced fertility, and a photosynthetic phenotype
111 correlated with increasing light intensity [27].

112 Identifying cyanobacterial rhomboid proteases was of interest because much of their
113 photosynthetic machinery is conserved in plant chloroplasts. As above, these oxygenic
114 photoautotrophs were already found to share some proteolytic mechanisms, but aquatic
115 cyanobacteria encounter distinct environmental challenges. One such is acquisition of carbon
116 dioxide, which diffuses poorly in water [28]. Cyanobacteria have overcome this constraint,
117 which coexists alongside the imperfect affinity of ribulose biphosphate carboxylase-
118 oxygenase (RubisCO) for CO₂ and its wasteful side reaction with oxygen [29], through the
119 evolution of a specialised CO₂-concentrating mechanism (CCM). Carboxysome 'organelles'
120 house the cyanobacterial RubisCO [30-32] and enrich the CO₂ environment. Because the
121 CCM is energy-dependent, it is regulated at multiple levels, including transcriptional control
122 of CO₂-uptake genes (for review, see [33]). Regulatory components include both activator
123 and repressor transcription factors [34] and, notably, proteolysis of the central NdhR
124 transcription factor (TF) by FtsH2 [35].

125 Here, mutant cells lacking the Slr1461 rhomboid protease were observed to aberrantly
126 regulate oxygen evolution during mixotrophic growth, when the need for carbon fixation
127 from CO₂ was reduced. The possibility of this rhomboid protease affecting regulation of the
128 CCM, in addition to activity of the FtsH protease, was considered by investigating
129 transcription of CCM TF genes, including NdhR, CmpR and an AbrB family member in
130 *Δslr1461 Synechocystis*. Whereas there was no indication of transporters being misregulated
131 at the level of steady-state mRNA, the *Δslr1461* rhomboid-null mutant exhibited altered
132 levels of TF transcripts when CO₂ concentrations were raised. There is increasing interest in
133 TF activated by proteolytic cleavage in other systems [36], and transcriptional links also
134 found between *slr1461* and *ftsH2* were intriguing when considered alongside a recent report
135 of a *Bacillus* bacterial rhomboid cooperating with FtsH in degradation of a transporter protein
136 [37]. This study of the *Synechocystis* rhomboid therefore adds a further protein regulator to
137 control networks for bacterial oxygenic photosynthesis and provides a route for further study
138 of coordinated proteolysis events.

139

140 **3. Methods**

141 **3.1 Inactivation of *Slr1461***

142 Glucose-tolerant (GT) *Synechocystis* sp. PCC 6803 cells from 25–50 ml cultures in
143 exponential growth phase (OD₇₅₀ ~0.5) were harvested by centrifugation, resuspended in 100
144 µl fresh BG11 medium [38] and mixed with 1–2 µg of plasmid DNA for insertional
145 inactivation by homologous recombination of an antibiotic-resistance gene-interrupted
146 *slr1461* open reading frame (ORF). Following incubation at 30 °C for 4 h at 8 µmol photons

147 $\text{m}^{-2} \text{s}^{-1}$ in a stationary illuminated incubator, with occasional inversion of the tube, cells were
148 plated onto non-selective BG11-agar and incubated overnight. After 24 h, plates were
149 overlaid with 3 ml of 0.6 % agar containing selection antibiotic (i.e., 15 μl of 100 mg ml^{-1}
150 kanamycin per 3 ml of 0.6 % agar). Antibiotic-resistant transformants were picked as single
151 colonies after ~ 2 weeks and plated on fresh selective agar plates at least twice to ensure
152 homoplasmy of the polyploid genome before confirming this by PCR (Supplementary
153 Figure 1). The pEERM4 vector (Addgene plasmid #64026), which integrates into the
154 chromosomal neutral site 2, was used to construct the *Slr1461* complementation plasmid.
155 pEERM4 plasmid contains a nickel-inducible *rnsB* promoter [39]. The full-length *slr1461*
156 coding sequence was cloned into pEERM4 using *XbaI* and *PstI* restriction endonucleases to
157 generate pEERM_Slr1461. This construct was subsequently transformed into the *$\Delta\text{slr1461}$*
158 mutant to enable integration at neutral site 2.

159

160 3.2 Oxygen evolution

161 *Synechocystis* 6803 (glucose-tolerant; GT) cells were harvested once they reached an OD_{750}
162 of ~ 0.4 - 0.5 by centrifuging at 2000 $\times g$ for 5 min at room temperature (22 $^{\circ}\text{C}$) and were then
163 adjusted to an OD_{750} of ~ 0.5 with fresh BG11 medium. For mixotrophic cultures, the pellet
164 was resuspended in fresh BG11 medium containing 5 mM glucose. NaHCO_3 was added, to a
165 final concentration of 10 mM, 5 min before the start of measurements. The rates of net O_2
166 evolution and dark respiration were then measured [40] at 30 $^{\circ}\text{C}$ using a Clark-type electrode
167 (Hansatech, Kings Lynn, UK [41]). Sodium dithionite was used to calibrate the electrode.
168 Actinic light was provided using a 650 nm red LED light. Variable light intensity was set for
169 0-2300 $\mu\text{mol photons m}^{-2} \text{s}^{-1}$. After an initial 30 min dark adaption, O_2 evolution was
170 measured for 5 min, followed by dark respiration for 20 min. The mean net rate of
171 photosynthesis was then determined from the oxygen gradient over 5 min. Dark respiration
172 was determined by following the same procedure, except that it was calculated with data
173 from the last 5 min of the 20-min experiment.

174

175 3.3 Room temperature fluorescence

176 Maximum quantum yield of PSII was measured using a Walz (Effeltrich, Germany) pulse-
177 amplitude modulation (PAM) 101 fluorimeter with the 101-ED emitter-detector unit. A Walz
178 liquid cell adaptor maintained at 30 $^{\circ}\text{C}$ was used to contain the sample. Actinic light was
179 white light (50 $\mu\text{mol photons m}^{-2} \text{s}^{-1}$) behind a 420 nm Corning 4-96 glass filter (cut-on
180 wavelength at 600 nm). Far-red light was provided by PAM-102. Prior to measurement, cells
181 were harvested as before and concentrated to 10 $\mu\text{g ml}^{-1}$ chlorophyll and dark adapted for 5
182 min. Minimum fluorescence (F_0) was determined by illuminating with measuring light (0.01
183 $\mu\text{mol photons m}^{-2} \text{s}^{-1}$). Maximum fluorescence (F_m) for dark-adapted state was determined
184 with a 0.8-s long saturation (4500 $\mu\text{mol photons m}^{-2} \text{s}^{-1}$) pulse delivered from a Schott
185 (Elmsford, USA) KL 1500 white light source. The actinic light was then switched on and a

186 second saturation pulse was applied after 5 min (F'_m). Finally, maximum fluorescence (F_m)
187 was determined following injection of DCMU [(3,4-dichlorophenyl)-1,1-dimethylurea] at a
188 10 μ M final concentration to inhibit electron transport from PSII while actinic light was
189 on[42].

190

191 3.4 Low-temperature fluorescence

192 77 K fluorescence emission spectra from the WT and Δ *slr1461* insertional inactivation
193 mutant were recorded in liquid nitrogen using Perkin Elmer (Waltham, MA, USA) LS 55
194 luminescence spectrometer. All samples were dark adapted for 5 min before freezing. The
195 excitation was 440 nm and 580 nm (5 nm slit width), and the fluorescence emission was
196 scanned in a wavelength range of 600–750 nm.

197

198 3.5 Growth assays

199 *Synechocystis* 6803 (GT) cultures were treated with 2.5 μ M NiCl₂ and incubated at 30 °C for
200 3 h with shaking to induce *slr1461* gene expression in the complemented strain. For
201 consistent growth conditions, the four replicates of WT and Δ *slr1461* cells were also treated
202 with 2.5 μ M NiCl₂ as above. The cells were then diluted approx. 22-fold to an OD₇₅₀ of 0.1
203 in 50 ml BG11 medium containing 5 mM glucose, and incubated at a light intensity of 16, 81
204 or 150 μ mol photons m⁻² s⁻¹ for ~6 days. A 1 ml sample was removed every 24 h for analysis.
205 Specific growth rate (μ) and doubling time (Td) of all cultures were calculated according to
206 the recorded OD₇₅₀ by the photospectrometer (Lambda U3900; Hitachi) according to:

207

$$208 \mu = \frac{\ln OD_t - \ln OD_0}{\Delta t}$$

$$209 Td = \frac{\ln 2}{\mu}$$

210 where OD_t and OD₀ refer to optical density at time t (h) and time zero, respectively.

211 Chlorophyll content was determined by subtracting the OD₇₅₀ nm value from the OD₆₈₀ nm
212 value and multiplying the result by 10.854, as previously described [43].

213

214 3.6 RNA isolation and quantitative real-time PCR

215 Four independent cultures of each strain were grown at a light intensity of 30 μ mol photons
216 m⁻² s⁻¹ in 'low' CO₂ (i.e., normal atmospheric levels) conditions to an OD₇₅₀ of 0.4-0.5.
217 Samples were either treated with 5 mM glucose (for mixotrophic growth), bubbled with 5 %
218 CO₂ (raised CO₂ condition), or left untreated (low CO₂ condition). After 6 h, 40 ml samples

219 were collected and pelleted at 3000 x g before being stored at -80 °C for RNA extraction.
220 Total RNA was extracted with Qiagen (Hilden, Germany) RNeasy Plant Mini kit. RNA was
221 treated with DNase I, RNase-free (Merck Life Sciences, Gillingham, UK) to eliminate
222 possible genomic DNA contamination. First strand cDNA was synthesised from 1 µg of RNA
223 with the RevertAid First Strand cDNA Synthesis Kit (Fisher Scientific, Loughborough, UK).
224 The cDNA was diluted 100-fold and 1 µl was used in quantitative RT-PCR, performed with
225 PowerUp (Applied Biosystems, Waltham, USA) SYBR green kit. The values for target genes
226 transcript level were normalised to both total RNA and to housekeeping gene *16S rRNA* (for
227 primer pairs, see Table 1), the relative changes in transcript abundance were analysed using
228 the $2^{-\Delta Ct}$ method [44, 45].

229

230 3.7 Sequence analysis

231 Sequence similarity searching was carried out with BLASTp and BLASTn using National
232 Center for Biotechnology Information (NCBI) public database (www.ncbi.nlm.nih.gov) [46].
233 Multiple alignments were generated with Clustal Omega [47] and alignments were edited
234 with Jalview [48]. Active site and expected transmembrane architecture were predicted using
235 hydropathy plots (TMHMM [49]) and AlphaFold3 [50].

236

237 4. Results

238 4.1 Identification of rhomboid proteases in cyanobacterial lineages

239 A single rhomboid protease encoded by the *Synechocystis* 6803 genome was identified from
240 sequence searches, and active site and expected transmembrane architecture were predicted
241 (Figure 1A-C). Almost all sequenced cyanobacterial genomes were found to encode a single
242 rhomboid (Figure 1D), but there was some notable variation, notably within the reduced
243 genomes of the *Prochlorococcus* genus. In contrast, the genome of *Acaryochloris marina*
244 MBIC 11017 includes six rhomboid protease genes, four were predicted for *Gloeothoece*
245 *citriiformis* PCC 7424 (also known as *Cyanothece* sp. PCC 7424) and *Leptolyngbya* sp. CCNP
246 1308, and three in *Trichormus variabilis* ATCC 29413 (previously named *Anabaena varibilis*
247 ATCC 29413), *Nostoc punctiforme* PCC 73102, *Crocospaera subtropica* ATCC 51142 and
248 *Picosynechococcus* sp. PCC 7002 (previously named *Synechococcus* sp. PCC
249 7002/*Agmenellum quadruplicatum* PR-6). In contrast, *P. marinus* str. MIT 9313 and *Rippkaea*
250 *orientalis* PCC 8801, were more typical of a fairly common subset predicted to have
251 duplicated rather than single rhomboid representatives. Examples of cyanobacterial genomes
252 that have reduced rapidly over evolution and lost their rhomboid gene were found to include
253 *Thermosynechococcus elongatus* BP-1, *Trichodesmium erythraeum* IMS101, and *P. marinus*
254 str. MIT 9312 and MIT 9211 [51], in tandem with a reduced complement of genes for
255 regulatory components such as sigma factors, required for transcription initiation, light
256 sensors/transducers and two-component sensor-kinases [51].

257

258 4.2 *Synechocystis* rhomboid sequence features

259 The *Synechocystis* 6803 rhomboid gene, ORF *slr1461*, translates to an amino acid sequence
260 with 37 % and 26 % identity to the *A. thaliana* chloroplast rhomboids At5g25752/RBL11 and
261 At1g25290/RBL10, respectively. It also shows 28 % identity with the endoplasmic
262 reticulum–localised At1g63120/RBL2, but no significant similarity was found with the
263 mitochondrial At5g38510/RBL9.

264 To predict whether the Slr1461 protein was likely to be enzymatically active or was an
265 inactive iRhom-type rhomboid, its sequence was aligned with representative enzymes already
266 experimentally verified to be catalytically active from *A. thaliana* [52], *H. sapiens* and *E. coli*
267 [53], and against the catalytically inactive *H. sapiens* iRhom2 rhomboid protease [54, 55]
268 (Figure 1A). The Slr1461 sequence aligned well with catalytically active rhomboids across
269 transmembrane domains, with clearly conserved active-site serine and histidine residues
270 (Figure 1A) [56]. These residues were similarly conserved in the active *A. thaliana* rhomboid
271 family (At1g63120/RBL2, mitochondrial At5g38510/RBL9 and chloroplast-located
272 At1g25290/RBL10), *H. sapiens* RHBDL2, and *E. coli* GlpG. Although the overall sequence
273 of human iRhom2 also aligned reasonably well (25 % identity between Slr1461 and iRhom2),
274 its corresponding positions lack these catalytic residues, consistent with iRhom2 known
275 enzymatic inactivity [18]. Slr1461 therefore displays features of the catalytically active
276 rhomboids. It is worthy of note, however, that it lacks a commonly conserved rhomboid N-
277 terminal tryptophan–tyrosine/arginine (W/YR) motif (Figure 1A and Supplementary Figure
278 2) [55, 57], which was hypothesised at one time to influence rate of proteolysis [58].

279

280 4.3 Photosynthesis phenotype

281 The *A. thaliana* chloroplast *RBL10* mutant's significantly higher NPQ values than in WT
282 plants, correlated with increasing light intensity [27], prompted exploration of a range of
283 photosynthetic parameters in Δ *slr1461* *Synechocystis*. Whole-cell absorbance spectra of
284 Δ *slr1461* and WT cells were broadly similar under low-intensity light (Figure 2) but spectra
285 normalised to the phycocyanin peak (635 nm) revealed a slightly higher absorbance at 687
286 nm in Δ *slr1461*, consistent with an increased chlorophyll a contribution relative to
287 phycobiliproteins. Quantification of pigment confirmed that Δ *slr1461* cultures contained
288 significantly higher total chlorophyll a than WT (Δ *slr1461* mean \pm SEM, 8.7 ± 0.51 μ M vs
289 WT 6.1 ± 0.08 μ M; t test $p = 0.024$, 7 d.f.), supported by ANOVA (see below; Table 3).
290 Oxygen evolution in low light-grown *Synechocystis* WT vs Δ *slr1461* cells was not
291 significantly different if cultures were grown in standard BG11 autotrophic medium with
292 saturating bicarbonate (Figure 3A). Likewise, the PAM fluorometry assays of Δ *slr1461*
293 Fv/Fm, PSII efficiency and NPQ produced measurements not significantly different from WT
294 under low-intensity light conditions (Table 2).

295 GT *Synechocystis* strains are useful for mutant studies because genes encoding key
296 photosynthetic components can be knocked out but cultures are able to remain viable [59] if
297 the BG11 defined medium is supplemented to permit heterotrophy. GT cells can therefore
298 acquire inorganic carbon either from CO₂ during autotrophic growth or, alternatively, from
299 both glucose and CO₂ in mixotrophic growth. The measurement of oxygen evolution rate
300 under such mixotrophic conditions revealed the most distinct phenotype for glucose-tolerant
301 *Δslr1461* *Synechocystis*. The rate of photosynthesis, previously identical in autotrophic
302 cultures of *Δslr1461* and WT (Figure 3A), was regulated down by about a third in WT cells
303 when grown mixotrophically, as expected. This reduction, however, did not occur in
304 mixotrophic *Δslr1461* cells (Figure 3B). Importantly, dark respiration rates were comparable
305 between the mutant and WT strains (Supplementary Figure 5), indicating that the observed
306 differences in O₂ evolution under mixotrophy reflected changes in photosynthetic regulation
307 rather than respiratory activity.

308 As cyanobacteria divide more rapidly in the presence of glucose [60], a marked difference
309 like this in photosynthetic activity (Figure 3B) might arise if there was a defect in glucose
310 import in the absence of the Slr1461 rhomboid. Growth rates of the strains did not suggest
311 altered nutrient acquisition, however: statistical analysis using two-way ANOVA (Table 3;
312 Supplementary Figure 4) confirmed that, whereas increasing light intensity significantly
313 affected both doubling time (F = 30, p = < 0.0001) and chlorophyll a content (F = 17, p = <
314 0.0001), the genotype (i.e., mutant vs WT) only influenced chlorophyll a (F = 51, p =
315 0.0001), with the lack of Slr1461 having little effect on doubling time (F = 3.2, p = 0.0551). A
316 check on experimental conditions showed there was no significant interaction between
317 genotype and light intensity, p > 0.12).

318

319 4.4 Genetic regulation of CO₂ concentration components

320 Mutant *Δslr1461* cells failed to downregulate photosynthesis under mixotrophic growth,
321 when a decrease in photosynthetic activity would normally be observed in *Synechocystis*
322 strains that are capable of heterotrophy. The reduced photosynthesis in WT GT cells follows a
323 decrease in the rate of bicarbonate uptake [61] and metabolic regulation that reduces the
324 activity of the carbon-fixing enzyme, RuBisCO [62]. A hypothesis that lack of Slr1461
325 resulted in altered behaviour of the CCM was therefore tested by quantifying the steady-state
326 mRNA of *slr1461* and of key CCM genes.

327 Whether the cyanobacterial rhomboid protease itself was regulated at the level of transcript
328 abundance under high CO₂ conditions was investigated by quantifying *slr1461* mRNA level
329 in WT *Synechocystis* (Figure 4A). *slr1461* transcript level did indeed increase when cultures
330 were bubbled with 5 % CO₂, when cells also had higher chlorophyll *a* content than did WT,
331 as noted previously (Table 3). These data indicated that the Slr1461 protease may be
332 involved in regulation of carbon assimilation.

333 Genes encoding components of the CCM were therefore tested during adaptation of *Δslr1461*
334 cultures to high CO₂ or to mixotrophic conditions, to assess their transcription levels when
335 carbon fixation demand was reduced (Figure 4; Supplementary Table 2). The *sbtA* gene,
336 encoding the Na⁺-dependent HCO₃⁻ transporter, was aberrantly low under all conditions in
337 *Δslr1461*: for example, the mutant had a log₂-fold *sbtA* level of -0.63 (p = 0.014) vs WT
338 under standard (lower) CO₂ conditions, moving to a -1.01 log₂-fold value (p = 0.015) under 5
339 % (raised) CO₂ (Figure 4B; Supplementary Tables 2, 3).

340 Also aberrant was the transcript for the NdhF3 protein, a component of the cyanobacterial
341 high affinity CO₂ uptake system (comprising a complex of NdhD3/D4 and NdhF3/F4), which
342 catalyses CO₂ uptake by converting CO₂ into HCO₃⁻. In this case, in mixotrophic *Δslr1461*
343 cultures, *ndhF3* mRNA levels in the mutant were similar to those in WT (Supplementary
344 Table 2). In autotrophy, however, under normal atmospheric CO₂ conditions, *ndhF3* mRNA
345 log₂-fold levels were -5.90, and in raised CO₂ were -4.57 (Figure 4A; Supplementary Table
346 2), i.e., lower than in *Δslr1461* than WT in both conditions. Likewise, *slr1461* itself had
347 been observed to accumulate only under raised CO₂, and not under mixotrophic glucose-
348 supplemented conditions (Figure 4A; Supplementary Table 2), a CO₂-dependent regulation of
349 *slr1461* was reported before [63]. Therefore, the lack of difference in *ndhF3* transcript level
350 between WT and *Δslr1461* mutant in mixotrophic growth can be attributed to the absence of
351 *slr1461* transcripts. When Slr1461 is not expressed (i.e., in mixotrophy), its regulatory
352 influence on NdhF3 expression is lost.

353 Other CCM components examined were CmpR and an AbrB family member. Both *abrB2* and
354 *cmpR* were also aberrantly regulated when Slr1461 was lacking, being significantly lower in
355 the *Δslr1461* mutant than WT when cultures were subject to increased CO₂ (Figure 4B,
356 Supplementary Table 2), although their levels were little different in *Δslr1461* to WT under
357 lower CO₂ levels.

358

359 **4.5 Co-ordinate control of CCM by proteases**

360 It was previously reported that induction of *ndhF3* and *sbtA* requires the FtsH2 protease as
361 these CCM transcripts were not upregulated under low CO₂ conditions in a null mutant with
362 inactivated *ftsH2* [35]. Meanwhile, increased *ftsH2* transcript levels have been reported in
363 response to oxidative stress; not to change in a shift from high to low CO₂ [35]; or with a
364 very minor upregulation in transcript under CO₂ downshift in an earlier study [63]. The
365 presence of the FtsH2 protease in networks connected with CCM regulation was further
366 monitored in WT compared with *Δslr1461* cells, comparing *ftsH2* transcript levels in standard
367 or raised CO₂ conditions in this mutant. Notably, after increasing CO₂ levels, the *ftsH2*
368 transcript level in *Δslr1461* remained lower than in WT cells (Figure 4B; Supplementary
369 Table 2), indicating that Slr1461 presence or proteolytic activity may affect induction of the
370 *ftsH2* gene in WT cyanobacteria.

371 To confirm that the decrease in CCM genes' transcript levels resulted from absence of
372 Slr1461 activity, the *slr1461* gene was used to complement Δ *slr1461* cells. In the
373 complemented line, *slr1461*, *ftsh2* and *ndhF3* transcript levels were rescued (Supplementary
374 Figure 6). The regulatory changes here suggested that further exploration is warranted, to
375 elucidate precisely the role of Slr1461 in connection with CCM processes.

376

377 5. Figures and tables

378 5.1 Tables

379 **Table 1. Primers pairs used in qRT-PCR and *slr1461* complementation**

For qRT-PCR:

slr1461_F: TCTTTGCACCCTTTCTCCAT
slr1461_R: TTTGGAACCAACCTCGAAAG

ftsH2_F: GCAAGTTAGCGACCCAGAAG
ftsH2_R: CCCACAAAACCCCAAACCAT

sbtA_F TGGTGCTCTGTATCCCTTTATG
sbtA_R TGCTGAACGATTCCCTCAATACT

ndhF3_F: TTTGGCCTTAATTGCTGGAC
ndhF3_R: GCGATCGCAATTAAAGAAGC

16S rRNA_F: CACACTGGGACTGAGACAC
16S rRNA_R: CTGCTGGCACGGAGTTAG

abrB2_F: CTGCCCCGGGTCAATATGAT
abrB2_R: TTGGATTGCACGCTAATGCG

cmpR_F: GTGATTGCTGACCTCCAGGG
cmpR_R: CCCAAAAGTCGTGGCACAAA

For complementation:

slr1461_F: CTCTAGACCACCATGAGCCAAAATTCC
slr1461_R: CTGCAGTGCTAATTTTGTCTGTAGTAATGC

380

381 2. Photosynthesis in the *Synechocystis* Δ *slr1461* rhomboid protease mutant

Autotrophic

Mixotrophic

High light autotrophic

Table	F_v/F_m	F_v/F_m DCMU	Φ_{PSII}	NPQ	F_v/F_m	F_v/F_m DCMU	Φ_{PSII}	NPQ	F_v/F_m	F_v/F_m DCMU	Φ_{PSII}	NPQ
Wild type	0.38 (±0.04)	0.56 (±0.01)	0.35 (±0.02)	0.25 (±0.02)	0.30 (±0.03)	0.49 (±0.01)	0.20 (±0.06)	0.13 (±0.06)	0.26 (±0.02)	0.32 (±0.02)	0.14 (±0.03)	0.09 (±0.01)
<i>Δslr1461</i>	0.37 (±0.02)	0.58 (±0.0)	0.37 (±0.04)	0.26 (±0.02)	0.32 (±0.04)	0.49 (±0.03)	0.17 (±0.06)	0.13 (±0.06)	0.31 (±0.00)	0.36 (±0.01)	0.13 (±0.01)	0.10 (±0.02)

382 Pulse-modulated chlorophyll fluorescence measurements of quantum yield of photosystem II (PSII):
383 photochemical quantum yield F_v/F_m for dark-adapted cells was calculated from $(F_m - F_0)/F_m$. Maximum quantum
384 yield of PSII (F_v/F_m DCMU) was measured using a protocol employing continuous illumination in the presence
385 of 10 μ M DCMU. The effective quantum yield of PSII (Φ_{PSII}) was calculated, $(F'_m - F_t)/F'_m$; and non-
386 photochemical quenching (NPQ) was calculated from $(F_m - F'_m)/F'_m$. Results are means from three biological
387 measurements \pm standard deviation.

388

389 **Table 3. Two-way ANOVA to analyse the effects of WT vs *Δslr1461* genotype and light**
390 **intensity, and their interaction, on doubling time and chlorophyll *a* (Chl *a*) content**

	Genotype			Light intensity			Genotype vs light intensity		
	Df	F	p	Df	F	p	Df	F	p
Doubling time	2	3.2	0.0551	2	30	<0.0001	4	1.9	0.1287
Chl <i>a</i>	2	51	<0.0001	2	17	<0.0001	4	1.0	0.3927

391 Data were transformed (log, square root, or reciprocal) as needed to meet linear model assumptions. Df, Degrees
392 of freedom; F, variation between sample means; p, significance levels.

393

394

395 **FIGURE 1. Slr1461 motifs for rhomboid catalytic activity.** (A) Slr1461 aligned with plant
396 and human rhomboid amino acid (aa) sequences. Colour, aa chemical properties and degree
397 of conservation (standard ClustalX scheme [47]: purple, acidic amino acids; blue,
398 hydrophobic; green, polar and neutral; brown, glycine; khaki, proline). Segments of
399 sequences aligned are from predicted full-length proteins as follows: *Synechocystis* Slr1461
400 aa27-196; *A. thaliana* enzymatically active rhomboids RBL2, aa64-252/ plastid RBL9,
401 aa275-375 /plastid RBL10, 128-310/ plastid RBL11, 85-272; *H. sapiens* catalytically active
402 RHBDL2, aa73-273; *H. sapiens* catalytically inactive iRhom2, aa605-796; and *E. coli* GlpG,
403 aa97-276. Bar above sequence alignment indicates conserved aa W/YR, S and H. (B)
404 Slr1461, Predicted transmembrane domains (TMHMM) [64]. (C) AlphaFold 3-predicted
405 structure of full-length *Synechocystis* sp. PCC 6803 Slr1461 protein[50]. (D) Distribution of
406 rhomboid proteases in cyanobacteria: unrooted phylogenetic tree for 16S rRNA generated
407 using the neighbour-joining method. The presence or absence of rhomboid (Rho) protein in
408 each cyanobacterial strain is shown on the right; "No Rho", absence of rhomboid protein.

409

410 **FIGURE 2. Photosystems and pigments in 77K fluorescence emission and absorption**
411 **spectra of mixotrophic wild type (WT) vs *Δslr1461* cells.** (A) 77K spectra normalised to
412 the emission band at 650 nm (580 nm excitation); (B) 77K spectra normalised to the emission
413 band at 725 nm (440 nm excitation); (C) absorption spectra normalised at 687 nm. Maximum
414 absorbance at 448 nm, 635 nm, and 687 nm corresponds to carotenoid, phycocyanin and
415 chlorophyll peaks, respectively. Cultures for A-C grown in BG11 medium supplemented with
416 5 mM glucose at 8 $\mu\text{mol photons m}^{-2} \text{s}^{-1}$ light. Green line, *Δslr1461*; purple line, WT
417 *Synechocystis* sp. PCC 6803.

418

419 **FIGURE 3. Light-response curve for wild type vs *Δslr1461* cells.** Oxygen evolution rate
420 versus photon flux density (PFD) for autotrophic (A) vs mixotrophic (B) cultures grown at 8
421 $\mu\text{mol photons m}^{-2} \text{s}^{-1}$ light. Cells grown mixotrophically were supplemented with 5 mM
422 glucose. Net photosynthesis rate (measured as in Methods) datapoints are the mean of three
423 measurements \pm SEM. For statistics, unpaired Student's t test was performed. Asterisks,
424 Statistically significant changes (P-value < 0.05).

425

426 **FIGURE 4. Effect of high CO₂ on CCM gene transcript level in (A) wild type (WT) or**
427 **(B, C) *Δslr1461* compared with WT.** Strains grown in atmospheric-level CO₂ (low CO₂) at
428 30 $\mu\text{mol photons m}^{-2} \text{s}^{-1}$ light intensity until OD₇₅₀ of 0.4-0.5 after which they were bubbled
429 with 5 % CO₂ (high CO₂) or left untreated before further 6 h incubation. qRT-PCR on
430 extracted RNA permitted calculation of expression levels relative to 16S rRNA reference
431 gene, with further normalisation to the WT (Figure 4B-C, Supplementary Table 2). Statistical
432 significance (*p*-value \leq 0.05), denoted by *, \leq 0.05; **, 0.01; ****, 0.0001. For a complete
433 list of *p*-values, see Supplementary Table. 3.

434

435 **FIGURE 5. Proposed further investigation of Slr1461 roles in adaptation of**
436 ***Synechocystis* to the environment.** (A) Under low CO₂ conditions, the oxygenase activity of
437 RuBisCO leads to accumulation of 2-phosphoglycolate (2-PG) in the cells [65]. Binding of 2-
438 PG to NdhR causes it to be released from the DNA, resulting in activated transcript level of
439 CCM genes [66]. Meanwhile, NdhR is not degraded in absence of FtsH2 [35]. (B) High CO₂
440 levels were correlated with increased transcript level of the *slr1461* gene, which is
441 hypothesised to enhance proteolysis of the rhomboid's as-yet unidentified, activated
442 substrate. This cleaving of the Slr1461-substrate(s) by Slr1461 protease is proposed as a
443 possible mechanism in the pathway for the observed upregulation of *ftsh2* transcript levels. At
444 the same time, 2-oxoglutarate (2-OG) accumulates under high CO₂-low nitrogen conditions:
445 binding of 2-OG to NdhR leads to NdhR to adopt a repressor conformation [66], resulting in
446 repression of CCM genes. (C) Resulting network of coordinated regulation of NdhR, CmpR
447 and AbrB2 by carbon and nitrogen metabolism. The 2-PG and 2-OG levels have opposite
448 effects on the activity of NdhR. Under low CO₂ conditions, the activity of RuBisCO shifts

449 predominantly to the oxygenation of ribulose-1,5-bisphosphate. This, in turn, causes the cell
 450 to accumulate 2-PG. 2-OG serves as an intermediate between carbon and nitrogen
 451 assimilation, but under high CO₂ conditions, the conversion of 2-OG with ammonium (NH₄⁺)
 452 into glutamate is low, resulting in 2-OG accumulation in the cell. The 2-OG and 2-PG
 453 molecules are denoted with ● and ●, respectively. Figure 5C was adapted from [66].

454

455

456

457

458

459

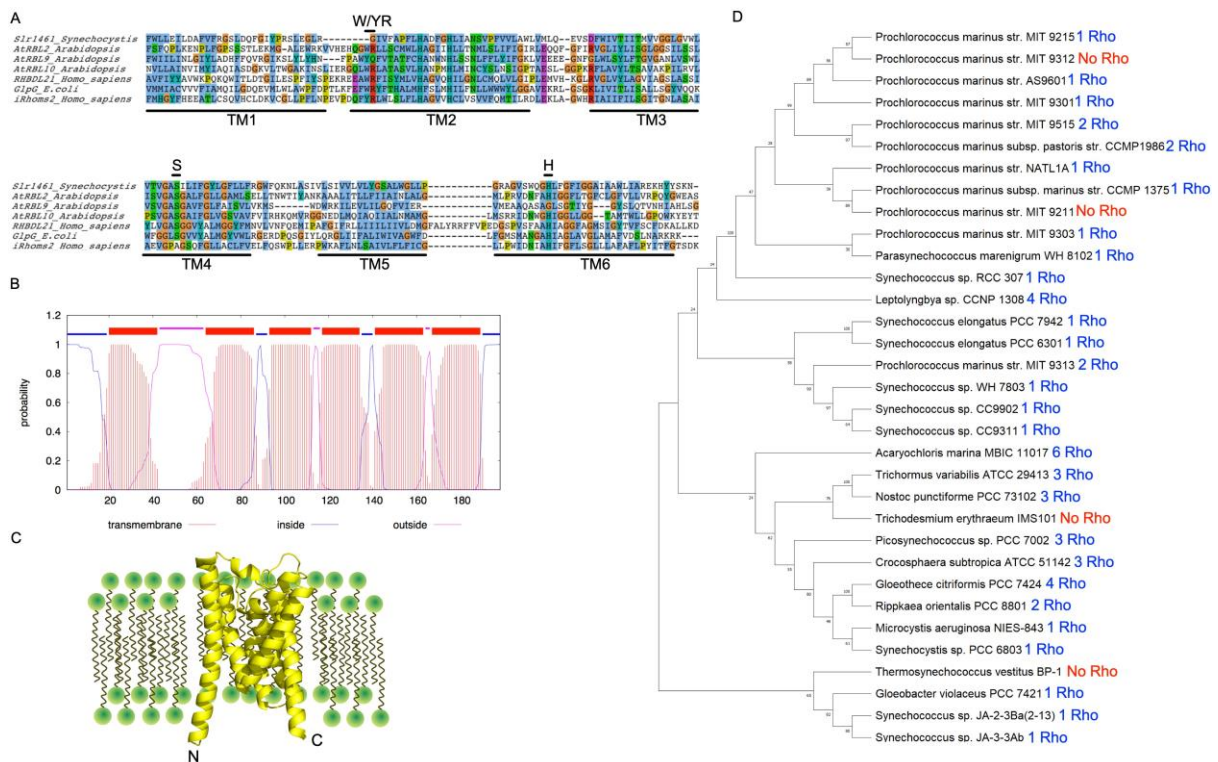
460

461

462 **FIGURE 1**

463

464



465

466

467

468

469

470

471

472

473

474

475

476

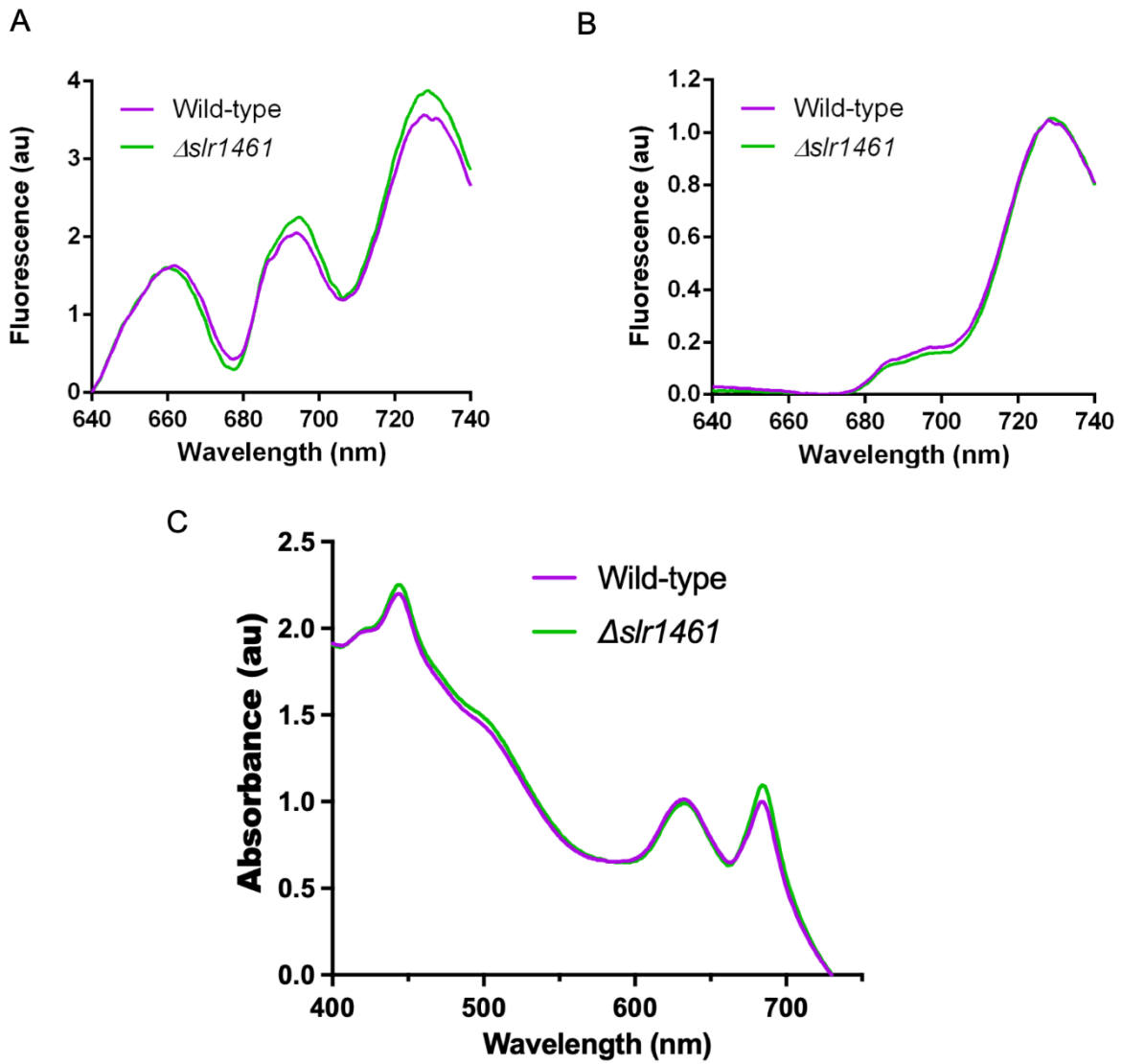
477

478

479

480

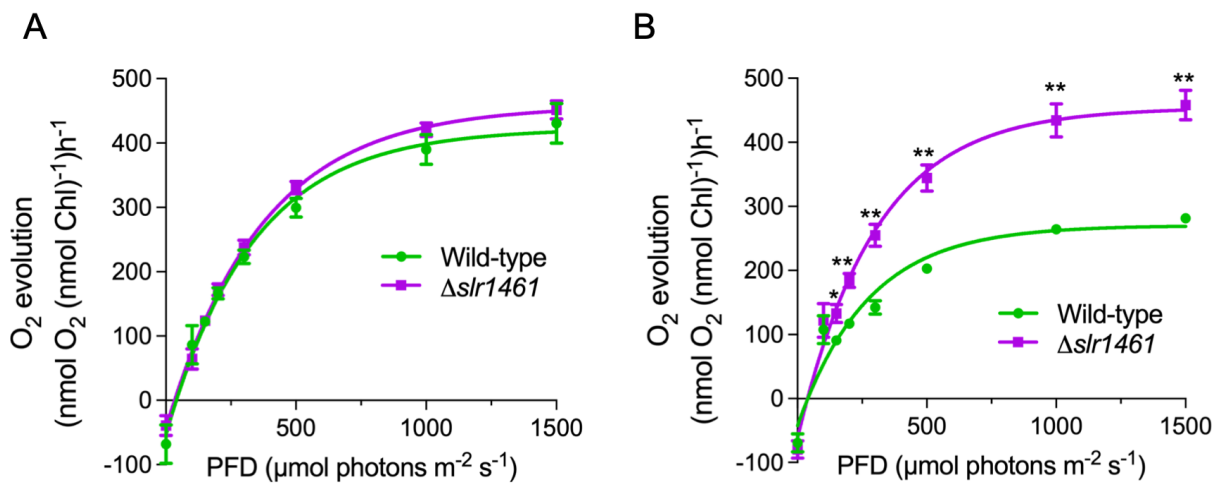
481 **FIGURE 2**



482

483 **FIGURE 3**

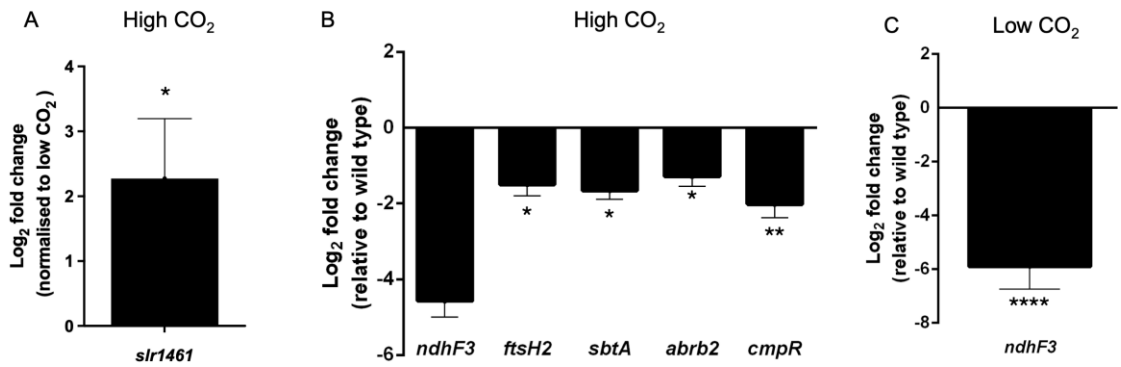
484



485

486 **FIGURE 4**

487

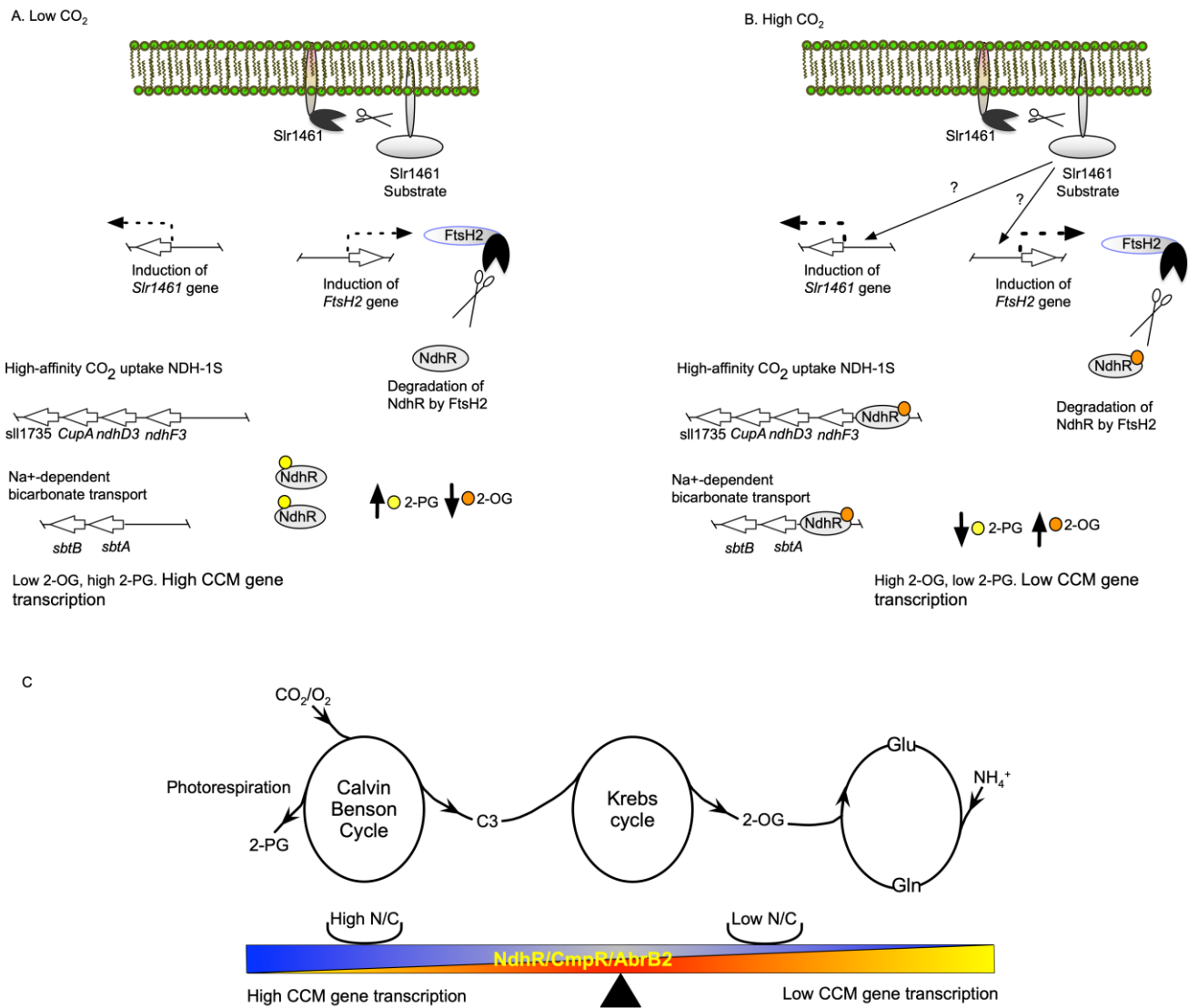


488

489

490 **FIGURE 5**

491



492

493 6. Discussion

494 Given their evolutionary relationship with plastids, cyanobacterial predicted rhomboid
495 proteases were examined (see Supplementary Figure 3) to compare features and conserved
496 photosynthesis-related roles. This first experimental investigation into the function of a
497 cyanobacterial rhomboid protease utilised the single rhomboid identified in the genome of the
498 model oxygenic photosynthetic prokaryote *Synechocystis*, with reference to the homologous
499 RBL10 protease of the *A. thaliana* chloroplast. Early literature upon discovery of this protein
500 family reported the most common occurrence in prokaryotic genomes was of a single
501 rhomboid enzyme, as identified in *Synechocystis*, but, subsequently, it has become clear there
502 are many cyanobacterial genera whose genomes encode multiple copies [67]. BLAST
503 searches of more recently sequenced genomes in fact found many bacteria with duplicated
504 rhomboid genes: the cyanobacterial genera documented here include those encoding as many
505 as six copies (Figure 1D). This mirrors another group of membrane proteases, where a single
506 FtsH protease regulates many processes in *E. coli* [7] in contrast with the four FtsH copies of
507 both *Synechococcus* sp. PCC 7502 and *Synechocystis* sp. PCC 6803 [20, 68, 69], whose
508 shared and specific roles are integral to oxygenic photosynthesis [20, 21]. Phylogenetic
509 analysis of rhomboid proteins in cyanobacteria showed that species encoding multiple
510 representatives have highly similar sequences indicative of gene duplication, except for the
511 *Acaryochloris marina* genome, which, despite the presence of six rhomboids, contains
512 divergent genes that appear more distinct from one another (Supplementary Figure 3).
513 Further dissection of the cyanobacterial single-copy versus multiple-copy rhomboids' roles
514 might provide insight into how a handful of organisms (such as *P. marinus* subspecies) have
515 been able to function without their rhomboid protease (Figure 1D) despite this protein
516 family's near-ubiquity across evolution.

517 The *Synechocystis* Slr1461 amino-acid sequence shows good overall alignment with other
518 organisms' rhomboid proteases that are known to be catalytically active. Slr1461 contains the
519 nucleophile Ser and acceptor His required for proteolytic attack of substrate (Figure 1) but it
520 lacks the W/YR motif often conserved near rhomboid proteases' N-termini (Figure 1A;
521 Supplementary Figure 2). This motif was initially postulated to play a role in substrate gating
522 but has since been ruled out as the mechanism of capture [58] and its link with enzymatic
523 activity is now questioned. As the presence of conserved active-site serine and histidine
524 suggest a catalytically active protease, this rhomboid may in fact be an interesting candidate
525 for investigations of rhomboid proteolysis in the presence or absence of the W/YR motif [70,
526 71]. The observed phenotypes here following the $\Delta slr1461$ insertional inactivation mutant
527 also support a hypothesis of Slr1461 being a proteolytically active enzyme, but it must be
528 noted that regulatory roles for inactive rhomboids have been shown to be plausible in bacteria
529 [72], since an 'adaptor' function was reported for the *Bacillus* enzyme when acting in concert
530 with an FtsH [37].

531 The constructed *Synechocystis* $\Delta slr1461$ mutant line was investigated for a range of
532 photosynthetic parameters because of the plastid membrane location of the homologous *A.*

533 *thaliana* rhomboid RBL10, and the *RBL10* null mutant's light-intensity-dependent raised
534 NPQ [27]. No dramatic difference was identified, however, in *Δslr1461* cells' pigment–
535 photosystem composition (Figure 2). Furthermore, there was no difference in NPQ under
536 light conditions tested (Table 2), despite that aspect of the *A. thaliana* RBL10-null phenotype.
537 The most dramatic difference observed with lack of Slr1461 was higher oxygen evolution
538 compared with WT when cells were grown mixotrophically, i.e., with insufficient glucose for
539 full heterotrophy (Figure 3B). Given that the *Bacillus* rhomboid-FtsH co-operative function
540 was reported to regulate a transporter, namely MgtE of *B. subtilis* [37], the question was
541 prompted over possible defective transport of glucose in the *Δslr1461* cells. Since glucose
542 typically increases growth rates and alters photosystem composition, the absence of any
543 significant difference in these parameters between mutant and WT cultures under
544 mixotrophic conditions (Table 3; Supplementary Figure 4) ruled out this possibility.

545 Since rhomboid proteases have often been reported to activate or release peptides involved in
546 signalling, the mis-regulation of *Δslr1461* carbon utilisation could result from a role for the
547 Slr1461 protease in activating the regulatory pathways that control the complex variations
548 needed for cyanobacterial CO₂ uptake and C fixing. It was reported before that numerous
549 CCM components' transcript levels respond to CO₂ [35, 63], which proved to be the case
550 here: several CCM-gene transcript levels were increased in WT cultures moved to high-CO₂
551 (Figure 4A), amongst them the *slr1461* transcript. Changes in levels tallied with those
552 reported previously when cells were moved from higher to lower CO₂ and with a small
553 *slr1461* transcript-level change found when the *ftsh2* transcript was upregulated [63]. To
554 integrate data from literature reports, further investigation of the magnitude and direction of
555 changes is needed, ensuring consistent and duplicated culture conditions and CO₂ levels.

556 Studies in prokaryotes to date only once implicated rhomboid proteases in regulation of
557 transcript levels [10], namely for the transcription factor (RipA, *cg1120*) involved in iron
558 homeostasis in *C. glutamicum* [10]. Certainly, the release of eukaryotic ER-bound
559 transcription factors is an attractive hypothesis for roles of this protease family, for which
560 some experimental evidence is accumulating [1, 73-75]. A relevant observation about
561 cyanobacterial carbon assimilation, then, was that the cAMP-regulated transcription factor
562 SyCRP1, which affects carboxysome formation (as well as many other pathways), can be
563 released from a membrane location [76]. That possible addition to the expanding CCM
564 regulatory map also supports a recent statement that, although the CCM is well characterised,
565 its regulation is complex and not yet fully understood [77].

566 A study in *Synechocystis* already showed that the FtsH2 protease was involved in the CCM
567 [35], in addition to its well-known role in turnover of the PSII D1 protein [20]. It was
568 proposed that this FtsH degrades the transcription factor, NdhR, that is required for induction
569 of CCM-genes [35]. It is notable how functional photosynthesis was required for induction of
570 CCM [34] in WT cells cultured in low CO₂ conditions, with the suggestion that oxidative
571 stress in the cells might enhance the expression of inducible CCM genes [35]. Conversely,
572 Haimovich-Dayana et al. (2011) reported that CCM genes were induced by glucose [78],

573 possibly though the previously mentioned cAMP-dependent transcription factor SyCRP1
574 [76].

575 qPCR assays here showed that loss of Slr1461 affected transcript levels of the high-affinity
576 CO₂ import system (Figure 4; Supplementary Table. 2), with CCM transport component and
577 *ftsH2* genes all misregulated. Whereas raising the CO₂ levels in cultures mildly repressed
578 CCM transcription in WT cells, a more marked reduction occurred in the Δ *slr1461* mutant
579 (Figure 4, Supplementary Table 2). A key observation is how transcript levels of the *ftsH2*
580 gene were affected by the absence of Slr1461, which raises the possibility that the role of the
581 rhomboid protease is to modulate the input of FtsH2 into CCM regulation. A hypothesis then
582 could be that Slr1461 action (its cleaved substrate or its own adaptor function) would permit
583 coordination of the cell's responses to mixotrophic growth and oxidative stress, i.e., an
584 upstream rhomboid protease fine-tunes FtsH regulation of the CCM. Results here (Figure 4;
585 Supplementary Table 2) suggested that this proposed Slr1461 activity would specifically
586 affect transcript levels under raised CO₂ conditions, potentially preventing excessive
587 downregulation of CCM genes. The relative position of the proteases and any rhomboid
588 substrate to CCM regulators requires further investigation (Figure 5). As raised CO₂ levels
589 regulated *slr1461* transcript level itself, that abiotic factor might likewise regulate availability
590 of a Slr1461-proteolysed substrate(s). Increased CO₂ in the scheme here could increase either
591 accessibility, degradation or activation of the unidentified Slr1461 substrate, which could
592 have upregulatory or downregulatory functions downstream. A scheme could be that
593 increased CO₂ results in increased transcript levels of *slr1461* and in Slr1461 cleaving its
594 substrate: this also increases the level of *ftsH2*. Notably, FtsH2 metalloprotease upregulation
595 can then increase transcript levels from CCM promoters in higher CO₂ because FtsH2
596 degrades the NdhR repressor protein [35]. Finally, it is worth mentioning that, since the *ftsH2*
597 gene is induced by oxidative stress in WT *Synechocystis* but not in the stress response
598 histidine kinase *hik33*⁻ mutant [35, 82], it would be of interest to explore how the kinase-
599 response regulator Hik33-RpaB abiotic stress mechanism interlinks with this extended CCM
600 regulatory network.

601 Better knowledge of how photosynthetic organisms respond to CO₂ increases may be useful,
602 underpinning future applications in the capture and storage of the rising CO₂ levels in the
603 atmosphere and oceans resulting from human activity. It has also been suggested that utilising
604 a cyanobacterial CCM in plants to improve Rubisco efficiency and hence crop yield might
605 not require changes to leaf anatomy [83]. This addition of control by Slr1461 to the FtsH2
606 release-from-repression of select CCM-related genes [35] would add a mechanism for
607 crosstalk and step-specific feedback. This echoes how proteases of the Clp and Deg families
608 supplement FtsH hetero-oligomers maintenance of functional PSII in varying environments,
609 which is augmented by phosphorylation controls from kinases and phosphatases [84, 85]. A
610 multilayered response mechanism might likewise be investigated for the CCM. Additionally,
611 as FtsH copies of type 'A' and 'B' can operate as heterodimers (namely FtsH2/3 and FtsH1/3
612 in *Synechocystis* [23, 86, 87]), another avenue of work would be to identify if upstream
613 Slr1461 rhomboid activity affects more than just the FtsH2 protease. As noted above, in the

614 case of the *B. subtilis*, the N-terminal cytosolic domain of rhomboid YqgP facilitates MgtE
615 transporter cleavage by FtsH, by an adaptor function that is separate from any catalytic
616 abilities [37]. Such united protease and pseudoprotease functions add to an increasing body of
617 evidence for proteases' ability to regulate cellular activities by a suite of mechanisms. The
618 diverse rhomboid functions reported to date lack a unifying and evolutionarily conserved
619 framework for their operation, but findings here for the CCM once again support linked roles
620 for rhomboid and FtsH membrane proteases. Further study of this aspect of the
621 cyanobacterial carbon-concentrating system may prove a useful focus for developing our
622 understanding.

623

624 **7. Author statements**

625 **7.1 Author contributions**

626 *IMI and EPT were responsible for design and analysis of experiments and project*
627 *management; IMI, DH, MBH, BTF, and EPT for conducting experiments; IMI and EPT*
628 *conceptualised and wrote the manuscript. All authors have read and agreed to the published*
629 *version of the manuscript.*

630

631 **7.2 Conflicts of interest**

632 *The author(s) declare that there are no conflicts of interest.*

633

634 **7.3 Funding information**

635 The University of Greenwich funded EPT, BTF, DH (VC Scholarship), MB and IMI, and by
636 Towson University for IMI.

637

638 **7.4 Acknowledgements**

639 We thank Professor C.W. Mullineaux for help with 77K fluorescence spectra; Dr C. Bateman
640 for help in constructing *Slr1461* knockouts; and Dr M. Rafiq for valuable discussions.

641

642 **8. References**

- 643 1. **Freeman M.** The rhomboid-like superfamily: molecular mechanisms and biological
644 roles. *Annu Rev Cell Dev Biol* 2014;30:235-254.
- 645 2. **Urban S, Lee JR, Freeman M.** Drosophila Rhomboid-1 defines a family of putative
646 intramembrane serine proteases. *Cell* 2001;107(2):173-182.

- 647 3. **Lee JR, Urban S, Garvey CF, Freeman M.** Regulated intracellular ligand transport and
648 proteolysis control EGF signal activation in Drosophila. *Cell* 2001;107(2):161-171.
- 649 4. **Rather P.** Role of rhomboid proteases in bacteria. *Biochim Biophys Acta*
650 2013;1828(12):2849-2854.
- 651 5. **Stevenson LG, Strisovsky K, Clemmer KM, Bhatt S, Freeman M et al.** Rhomboid
652 protease AarA mediates quorum-sensing in *Providencia stuartii* by activating TatA of the
653 twin-arginine translocase. *P Natl Acad Sci USA* 2007;104(3):1003-1008.
- 654 6. **Ekici OD, Paetzel M, Dalbey RE.** Unconventional serine proteases: Variations on the
655 catalytic Ser/His/Asp triad configuration. *Protein Sci* 2008;17(12):2023-2037.
- 656 7. **Tomoyasu T, Gamer J, Bukau B, Kanemori M, Mori H et al.** *Escherichia coli* FtsH is a
657 membrane-bound, ATP-dependent protease which degrades the heat-shock transcription
658 factor sigma 32. *The EMBO Journal* 1995;14(11):2551-2460.
- 659 8. **Russell CW, Richards AC, Chang AS, Mulvey MA.** The Rhomboid Protease GlpG
660 Promotes the Persistence of Extraintestinal Pathogenic *Escherichia coli* within the Gut. *Infect*
661 *Immun* 2017;85(6).
- 662 9. **Lu J, Arutyunova E, Hartley B, Wong J, Chung H et al.** Rhomboid protease GlpG
663 regulates type 1 pili quality control and virulence in pathogenic *E. coli*. *Nat Commun* 2025.
- 664 10. **Luenenschloss A, Ter Veld F, Albaum SP, Neddermann TM, Wendisch VF et al.**
665 Functional Genomics Uncovers Pleiotropic Role of Rhomboids in *Corynebacterium*
666 *glutamicum*. *Front Microbiol* 2022;13:771968.
- 667 11. **Liu G, Beaton SE, Grieve AG, Evans R, Rogers M et al.** Bacterial rhomboid proteases
668 mediate quality control of orphan membrane proteins. *The EMBO journal*
669 2020;39(10):e102922.
- 670 12. **Hill RB, Pellegrini L.** The PARL family of mitochondrial rhomboid proteases. *Semin*
671 *Cell Dev Biol* 2010;21(6):582-592.
- 672 13. **McQuibban GA, Lee JR, Zheng L, Juusola M, Freeman M.** Normal mitochondrial
673 dynamics requires rhomboid-7 and affects *Drosophila* lifespan and neuronal function. *Curr*
674 *Biol* 2006;16(10):982-989.
- 675 14. **Lysyk L, Brassard R, Touret N, Lemieux MJ.** PARL Protease: A Glimpse at
676 Intramembrane Proteolysis in the Inner Mitochondrial Membrane. *J Mol Biol*
677 2020;432(18):5052-5062.
- 678 15. **Lin JW, Meireles P, Prudêncio M, Engelmann S, Annoura T et al.** Loss-of-function
679 analyses defines vital and redundant functions of the *Plasmodium* rhomboid protease
680 family. *Mol Microbiol* 2013;88(2):318-338.
- 681 16. **Santos JM, Ferguson DJ, Blackman MJ, Soldati-Favre D.** Intramembrane cleavage of
682 AMA1 triggers *Toxoplasma* to switch from an invasive to a replicative mode. *Science*
683 2011;331(6016):473-477.
- 684 17. **Zettl M, Adrain C, Strisovsky K, Lastun V, Freeman M.** Rhomboid Family
685 Pseudoproteases Use the ER Quality Control Machinery to Regulate Intercellular Signaling.
686 *Cell* 2011;145(1):79-91.
- 687 18. **Adrain C, Zettl M, Christova Y, Taylor N, Freeman M.** Tumor Necrosis Factor Signaling
688 Requires iRhom2 to Promote Trafficking and Activation of TACE. *Science*
689 2012;335(6065):225-228.
- 690 19. **Tripathi LP, Sowdhamini R.** Cross genome comparisons of serine proteases in
691 *Arabidopsis* and rice. *Bmc Genomics* 2006;7.

- 692 20. **Silva P, Thompson E, Bailey S, Kruse O, Mullineaux CW et al.** FtsH is involved in the
693 early stages of repair of photosystem II in *Synechocystis* sp PCC 6803. *The Plant cell*
694 2003;15(9):2152-2164.
- 695 21. **Bailey S, Thompson E, Nixon PJ, Horton P, Mullineaux CW et al.** A critical role for the
696 Var2 FtsH homologue of *Arabidopsis thaliana* in the photosystem II repair cycle in vivo. *J Biol*
697 *Chem* 2002;277(3):2006-2011.
- 698 22. **Friso G, Giacomelli L, Ytterberg AJ, Peltier JB, Rudella A et al.** In-depth analysis of
699 the thylakoid membrane proteome of *Arabidopsis thaliana* chloroplasts: new proteins, new
700 functions, and a plastid proteome database. *The Plant cell* 2004;16(2):478-499.
- 701 23. **Zaltsman A, Ori N, Adam Z.** Two types of FtsH protease subunits are required for
702 chloroplast biogenesis and Photosystem II repair in *Arabidopsis*. *The Plant cell*
703 2005;17(10):2782-2790.
- 704 24. **Kanaoka MM, Urban S, Freeman M, Okada K.** An *Arabidopsis* Rhomboid homolog is
705 an intramembrane protease in plants. *FEBS letters* 2005;579(25):5723-5728.
- 706 25. **Kmiec-Wisniewska B, Krumpe K, Urantowka A, Sakamoto W, Pratje E et al.** Plant
707 mitochondrial rhomboid, AtRBL12, has different substrate specificity from its yeast
708 counterpart. *Plant Mol Biol* 2008;68(1-2):159-171.
- 709 26. **Karakasis K, Taylor D, Ko K.** Uncovering a Link between a Plastid Translocon
710 Component and Rhomboid Proteases Using Yeast Mitochondria-Based Assays. *Plant and Cell*
711 *Physiology* 2007;48(4):655-661.
- 712 27. **Thompson EP, Smith SG, Glover BJ.** An *Arabidopsis* rhomboid protease has roles in
713 the chloroplast and in flower development. *Journal of Experimental Botany*
714 2012;63(10):3559-3570.
- 715 28. **Moroney JV, Ynalvez RA.** Proposed carbon dioxide concentrating mechanism in
716 *Chlamydomonas reinhardtii*. *Eukaryotic cell* 2007;6(8):1251-1259.
- 717 29. **Moroney JV, Somanchi A.** How do algae concentrate CO₂ to increase the efficiency
718 of photosynthetic carbon fixation? *Plant Physiol* 1999;119(1):9-16.
- 719 30. **Giordano M, Beardall J, Raven JA.** CO₂ concentrating mechanisms in algae:
720 Mechanisms, environmental modulation, and evolution. *Annu Rev Plant Biol* 2005;56:99-
721 131.
- 722 31. **Kaplan A, Schwarz R, Liemanhurwitz J, Reinhold L.** Physiological and Molecular
723 Aspects of the Inorganic Carbon-Concentrating Mechanism in Cyanobacteria. *Plant Physiol*
724 1991;97(3):851-855.
- 725 32. **Price GD, Badger MR, Woodger FJ, Long BM.** Advances in understanding the
726 cyanobacterial CO₂-concentrating-mechanism (CCM): functional components, Ci
727 transporters, diversity, genetic regulation and prospects for engineering into plants. *Journal*
728 *of experimental botany* 2008;59(7):1441-1461.
- 729 33. **Wang H-L, Postier BL, Burnap RL.** Alterations in Global Patterns of Gene Expression in
730 *Synechocystis* sp. PCC 6803 in Response to Inorganic Carbon Limitation and the Inactivation
731 of ndhR, a LysR Family Regulator. *Journal of Biological Chemistry* 2004;279(7):5739-5751.
- 732 34. **Daley SM, Kappell AD, Carrick MJ, Burnap RL.** Regulation of the cyanobacterial CO₂-
733 concentrating mechanism involves internal sensing of NADP⁺ and alpha-ketogutarate levels
734 by transcription factor CcmR. *PloS one* 2012;7(7):e41286.
- 735 35. **Zhang PP, Sicora CI, Vorontsova N, Allahverdlyeva Y, Battchikova N et al.** FtsH
736 protease is required for induction of inorganic carbon acquisition complexes in *Synechocystis*
737 sp PCC 6803. *Molecular Microbiology* 2007;65(3):728-740.

- 738 36. **Jarvis P, López-Juez E.** Biogenesis and homeostasis of chloroplasts and other plastids.
739 *Nat Rev Mol Cell Bio* 2013;14(12):787-802.
- 740 37. **Began J, Cordier B, Březinová J, Delisle J, Hexnerová R et al.** Rhomboid
741 intramembrane protease YqgP licenses bacterial membrane protein quality control as
742 adaptor of FtsH AAA protease. *Embo j* 2020;39(10):e102935.
- 743 38. **Castenholz RW.** Culturing methods for cyanobacteria. *Methods in Enzymology:*
744 Academic Press; 1988. pp. 68-93.
- 745 39. **Englund E, Andersen-Ranberg J, Miao R, Hamberger B, Lindberg P.** Metabolic
746 Engineering of *Synechocystis* sp. PCC 6803 for Production of the Plant Diterpenoid Manoyl
747 Oxide. *ACS Synth Biol* 2015;4(12):1270-1278.
- 748 40. **Brindley C, Acien FG, Fernandez-Sevilla JM.** The Oxygen Evolution Methodology
749 Affects Photosynthetic Rate Measurements of Microalgae in Well-Defined Light Regimes.
750 *Biotechnol Bioeng* 2010;106(2):228-237.
- 751 41. **Delieu T, Walker DA.** Improved Cathode for Measurement of Photosynthetic Oxygen
752 Evolution by Isolated Chloroplasts. *New Phytol* 1972;71(2):201-&.
- 753 42. **Campbell D, Hurry V, Clarke AK, Gustafsson P, Oquist G.** Chlorophyll fluorescence
754 analysis of cyanobacterial photosynthesis and acclimation. *Microbiol Mol Biol Rev*
755 1998;62(3):667-683.
- 756 43. **Lea-Smith DJ, Ross N, Zori M, Bendall DS, Dennis JS et al.** Thylakoid terminal
757 oxidases are essential for the cyanobacterium *Synechocystis* sp. PCC 6803 to survive rapidly
758 changing light intensities. *Plant Physiol* 2013;162(1):484-495.
- 759 44. **Andersen CL, Jensen JL, Ørntoft TF.** Normalization of real-time quantitative reverse
760 transcription-PCR data: a model-based variance estimation approach to identify genes suited
761 for normalization, applied to bladder and colon cancer data sets. *Cancer Res*
762 2004;64(15):5245-5250.
- 763 45. **Vandesompele J, De Preter K, Pattyn F, Poppe B, Van Roy N et al.** Accurate
764 normalization of real-time quantitative RT-PCR data by geometric averaging of multiple
765 internal control genes. *Genome Biol* 2002;3(7):Research0034.
- 766 46. **Altschul SF, Gish W, Miller W, Myers EW, Lipman DJ.** Basic local alignment search
767 tool. *Journal of Molecular Biology* 1990;215(3):403-410.
- 768 47. **Chenna R, Sugawara H, Koike T, Lopez R, Gibson TJ et al.** Multiple sequence
769 alignment with the Clustal series of programs. *Nucleic Acids Res* 2003;31(13):3497-3500.
- 770 48. **Clamp M, Cuff J, Searle SM, Barton GJ.** The Jalview Java alignment editor.
771 *Bioinformatics* 2004;20(3):426-427.
- 772 49. **Krogh A, Larsson B, G.V H, Sonnhammer EL.** Predicting Transmembrane Protein
773 Topology with a Hidden Markov Model: Application to Complete Genomes. *Journal of*
774 *Molecular Biology* 2001;305(3):567-580.
- 775 50. **Abramson J, Adler J, Dunger J, Evans R, Green T et al.** Accurate structure prediction
776 of biomolecular interactions with AlphaFold 3. *Nature* 2024;630(8016):493-500.
- 777 51. **Rocap G, Larimer FW, Lamerdin J, Malfatti S, Chain P et al.** Genome divergence in
778 two *Prochlorococcus* ecotypes reflects oceanic niche differentiation. *Nature*
779 2003;424(6952):1042-1047.
- 780 52. **Lavell A, Smith M, Xu Y, Froehlich JE, De La Mora C et al.** Proteins associated with
781 the *Arabidopsis thaliana* plastid rhomboid-like protein RBL10. *Plant J* 2021;108(5):1332-
782 1345.

- 783 53. **Wang Y, Zhang Y, Ha Y.** Crystal structure of a rhomboid family intramembrane
784 protease. *Nature* 2006;444(7116):179-180.
- 785 54. **Adrain C, Strisovsky K, Zettl M, Hu L, Lemberg MK et al.** Mammalian EGF receptor
786 activation by the rhomboid protease RHBDL2. *EMBO Rep* 2011;12(5):421-427.
- 787 55. **Lemberg MK, Freeman M.** Functional and evolutionary implications of enhanced
788 genomic analysis of rhomboid intramembrane proteases. *Genome Res* 2007;17(11):1634-
789 1646.
- 790 56. **Lemieux MJ, Fischer SJ, Cherney MM, Bateman KS, James MN.** The crystal structure
791 of the rhomboid peptidase from *Haemophilus influenzae* provides insight into
792 intramembrane proteolysis. *Proc Natl Acad Sci U S A* 2007;104(3):750-754.
- 793 57. **Bergbold N, Lemberg MK.** Emerging role of rhomboid family proteins in mammalian
794 biology and disease. *Biochim Biophys Acta* 2013;1828(12):2840-2848.
- 795 58. **Zoll S, Stanchev S, Began J, Skerle J, Lepsik M et al.** Substrate binding and specificity
796 of rhomboid intramembrane protease revealed by substrate-peptide complex structures.
797 *The EMBO journal* 2014;33(20):2408-2421.
- 798 59. **Jansson C, Debus RJ, Osiewacz HD, Gurevitz M, McIntosh L.** Construction of an
799 Obligate Photoheterotrophic Mutant of the Cyanobacterium *Synechocystis* 6803 1:
800 Inactivation of the *psbA* Gene Family. *Plant Physiol* 1987;85(4):1021-1025.
- 801 60. **Lee T-C, Xiong W, Paddock T, Carrieri D, Chang I-F et al.** Engineered xylose utilization
802 enhances bio-products productivity in the cyanobacterium *Synechocystis* sp. PCC 6803.
803 *Metabolic Engineering* 2015;30:179-189.
- 804 61. **Boye SA, Silman NJ, Mann NH, Carr NG.** Bicarbonate Concentration by
805 *Synechocystis* Pcc6803 - Modulation of Protein-Phosphorylation and Inorganic Carbon
806 Transport by Glucose. *Plant Physiol* 1992;99(2):601-606.
- 807 62. **Nieva M, Valiente EF.** Inorganic carbon transport and fixation in cells of *Anabaena*
808 *variabilis* adapted to mixotrophic conditions. *Plant and Cell Physiology* 1996;37(1):1-7.
- 809 63. **Wang HL, Postier BL, Burnap RL.** Alterations in global patterns of gene expression in
810 *Synechocystis* sp. PCC 6803 in response to inorganic carbon limitation and the inactivation of
811 *ndhR*, a LysR family regulator. *J Biol Chem* 2004;279(7):5739-5751.
- 812 64. **Krogh A, Larsson B, von Heijne G, Sonnhammer EL.** Predicting transmembrane
813 protein topology with a hidden Markov model: application to complete genomes. *J Mol Biol*
814 2001;305(3):567-580.
- 815 65. **Burnap RL, Hagemann M, Kaplan A.** Regulation of CO₂ Concentrating Mechanism in
816 Cyanobacteria. *Life (Basel)* 2015;5(1):348-371.
- 817 66. **Jiang YL, Wang XP, Sun H, Han SJ, Li WF et al.** Coordinating carbon and nitrogen
818 metabolic signaling through the cyanobacterial global repressor *NdhR*. *Proc Natl Acad Sci U S*
819 *A* 2018;115(2):403-408.
- 820 67. **Koonin EV, Makarova KS, Rogozin IB, Davidovic L, Letellier MC et al.** The rhomboids:
821 a nearly ubiquitous family of intramembrane serine proteases that probably evolved by
822 multiple ancient horizontal gene transfers. *Genome Biol* 2003;4(3):R19.
- 823 68. **Mann N, Novac N, Mullineaux C, Newman J, Bailey S et al.** Involvement of an FtsH
824 homologue in the assembly of functional photosystem I in the cyanobacterium
825 *Synechocystis* sp. PCC 6803. *FEBS letters* 2000;479:72-77.
- 826 69. **Shao S, Cardona T, Nixon PJ.** Early emergence of the FtsH proteases involved in
827 photosystem II repair. *Photosynthetica* 2018;56(1):163-177.

- 828 70. **Wang Y, Maegawa S, Akiyama Y, Ha Y.** The role of L1 loop in the mechanism of
829 rhomboid intramembrane protease GlpG. *J Mol Biol* 2007;374(4):1104-1113.
- 830 71. **Baker RP, Young K, Feng L, Shi Y, Urban S.** Enzymatic analysis of a rhomboid
831 intramembrane protease implicates transmembrane helix 5 as the lateral substrate gate.
832 *Proc Natl Acad Sci U S A* 2007;104(20):8257-8262.
- 833 72. **Adrain C, Cavadas M.** The complex life of rhomboid pseudoproteases. *Febs j*
834 2020;287(19):4261-4283.
- 835 73. **Guichard A, Biehs B, Sturtevant MA, Wickline L, Chacko J et al.** rhomboid and Star
836 interact synergistically to promote EGFR/MAPK signaling during Drosophila wing vein
837 development. *Development* 1999;126:2663-2676.
- 838 74. **Han SI, Nakakuki M, Nakagawa Y, Wang Y, Araki M et al.** Rhomboid protease
839 RHBDL4/RHBDD1 cleaves SREBP-1c at endoplasmic reticulum monitoring and regulating
840 fatty acids. *PNAS Nexus* 2023;2(11):pgad351.
- 841 75. **Eysholdt-Derzsó E, Renziehausen T, Frings S, Frohn S, von Bongartz K et al.**
842 Endoplasmic reticulum-bound ANAC013 factor is cleaved by RHOMBOID-LIKE 2 during the
843 initial response to hypoxia in Arabidopsis thaliana. *Proc Natl Acad Sci U S A*
844 2023;120(11):e2221308120.
- 845 76. **Bantu L, Chauhan S, Srikumar A, Hirakawa Y, Suzuki I et al.** A membrane-bound
846 cAMP receptor protein, SyCRP1 mediates inorganic carbon response in Synechocystis sp.
847 PCC 6803. *Biochim Biophys Acta Gene Regul Mech* 2022;1865(3):194803.
- 848 77. **Kurkela J, Tyystjärvi T.** Inorganic carbon sensing and signalling in cyanobacteria.
849 *Physiologia Plantarum* 2024;176(1).
- 850 78. **Haimovich-Dayana M, Kahlon S, Hihara Y, Hagemann M, Ogawa T et al.** Cross-talk
851 between photomixotrophic growth and CO₂-concentrating mechanism in Synechocystis
852 sp. strain PCC 6803. *Environ Microbiol* 2011;13(7):1767-1777.
- 853 79. **Bier E, Jan LY, Jan YN.** Rhomboid, a Gene Required for Dorsoventral Axis
854 Establishment and Peripheral Nervous-System Development in Drosophila-Melanogaster.
855 *Gene Dev* 1990;4(2):190-203.
- 856 80. **Freeman M, Kimmel BE, Rubin GM.** Identifying Targets of the Rough Homeobox
857 Gene of Drosophila - Evidence That Rhomboid Functions in Eye Development. *Development*
858 1992;116(2):335-&.
- 859 81. **Lage P, Jan YN, Jarman AP.** Requirement for EGF receptor signalling in neural
860 recruitment during formation of Drosophila chordotonal sense organ clusters. *Curr Biol*
861 1997;7(3):166-175.
- 862 82. **Kanesaki Y, Yamamoto H, Paithoonrangsarid K, Shoumskaya M, Suzuki I et al.**
863 Histidine kinases play important roles in the perception and signal transduction of hydrogen
864 peroxide in the cyanobacterium, Synechocystis sp. PCC 6803. *Plant Journal* 2007;49(2):313-
865 324.
- 866 83. **McGrath JM, Long SP.** Can the cyanobacterial carbon-concentrating mechanism
867 increase photosynthesis in crop species? A theoretical analysis. *Plant Physiol*
868 2014;164(4):2247-2261.
- 869 84. **Srivastava A, Shukla P.** Tightening the Screws on PsbA in Cyanobacteria. *Trends*
870 *Genet* 2021;37(3):211-215.
- 871 85. **Yi L, Liu B, Nixon PJ, Yu J, Chen F.** Recent Advances in Understanding the Structural
872 and Functional Evolution of FtsH Proteases. *Front Plant Sci* 2022;13:837528.

- 873 86. **Yu F, Park S, Rodermel SR.** The Arabidopsis FtsH metalloprotease gene family:
874 interchangeability of subunits in chloroplast oligomeric complexes. *Plant Journal*
875 2004;37(6):864-876.
- 876 87. **Boehm M, Yu J, Krynicka V, Barker M, Tichy M et al.** Subunit organization of a
877 synechocystis hetero-oligomeric thylakoid FtsH complex involved in photosystem II repair.
878 *The Plant cell* 2012;24(9):3669-3683.
- 879